Mechanical Systems and Signal Processing 179 (2022) 109405

Contents lists available at ScienceDirect

Mechanical Systems and Signal Processing

journal homepage: www.elsevier.com/locate/ymssp

Evaluation of modal identification under base motion excitation using vision techniques

Ángel J. Molina-Viedma [a,*], Luis Felipe-Sesé [a], Manuel Pastor-Cintas [a], Elías López-Alba [b], Francisco A. Díaz [b]

[a] Departamento de Ingeniería Mecánica y Minera, Campus Científico Tecnológico de Linares, Universidad de Jaén, 23700 Linares, Spain
[b] Departamento de Ingeniería Mecánica y Minera, Campus Las Lagunillas, Universidad de Jaén, 23071 Jaén, Spain

ARTICLE INFO

Communicated by: Janko Slavič

Keywords:
Base excitation
Vision techniques
3D-DIC
Transmissibility functions
Modal analysis

ABSTRACT

In certain situations, employing a movable base acting as the excitation of a mechanical system is the best or even the only way to determine the response model for modal analysis. However, the obtained transmissibility functions must be modified prior to modal identification with a conventional procedure based on frequency response functions. Moreover, when employing vision techniques, the response curves are noisier and even poorly defined as the sensitivity is significantly lower than traditional sensors. Using the right model for curve-fitting is particularly relevant in this case. The current study performs an analysis of the adaptation of transmissibility functions, obtained by a vision technique, to improve the accuracy of the modal data estimation with conventional procedures. Two sets of transmissibility functions were evaluated: the originally obtained in the experiment, and the adapted one. After modal identification, significant differences were found concerning mode shapes and curve synthesis. The adaptation improved the accuracy of the identification in all the measurement points, proved by statistical indicators of the curve-fitting procedure like the correlation coefficient and the error between the synthesised and the experimental curves.

1. Introduction

Vision techniques have attracted the attention of the scientific community in vibration and modal analysis thanks to the development of high-speed cameras technology, which makes them suitable for dynamic events, in general. The main benefit of these novel methodologies lies in the contactless full observation of the specimen surface, which does not alter the mechanical behaviour of the system. With appropriate image processing, a full-field measurement can be obtained, representing an extremely high-density grid of virtual sensors, i.e., measurement points. This spatial resolution is not reachable by any other system. Moreover, the setup is simpler compared to a high, but still limited, number of sensors required with traditional methods. This increases costs in sensors and acquisition systems, test preparation and probability of equipment malfunctioning. Hence, the scientific community highlights the rich information obtained with vision techniques, which provide both alternative and complementary tools in modal analysis [1], quite useful for model updating [2,3].

Among different techniques such as point tracking, optical flow or phase-based motion extraction, digital image correlation (DIC)

* Corresponding author.
E-mail address: ajmolina@ujaen.es (Á.J. Molina-Viedma).

https://doi.org/10.1016/j.ymssp.2022.109405
Received 4 April 2022; Received in revised form 24 May 2022; Accepted 4 June 2022
Available online 11 June 2022

outstands significantly. This technique is versatile, commercially available and its accurateness has been demonstrated in multiple fields of experimental mechanics. Besides, whereas most vision techniques are limited to two-dimensional motion analysis, occurring in a focused plane parallel to the camera sensor, DIC is suitable for stereoscopic systems to perform three-dimensional displacement measurements [4]. This technique has been widely employed for full-field modal analysis, using both simplified single-degree-of-freedom [5] and multi-degree-of-freedom procedures [6–8], and also for operational modal analysis [9–12].

Overall, validation studies have proved that the sensitivity of vision techniques is comparatively much lower to conventional techniques and transducers employed in modal analysis, such as accelerometers or laser vibrometry [13,14]. In those studies, the influence of noise in signals obtained for modal analysis is observed. Typically, the peak response of resonances is well characterised by these techniques, but valley response or anti-resonances are poorly-defined or even truncated by the noise floor. Moreover, as vision techniques are sensitive to displacements, they are usually more suitable for low frequencies. Despite that, Javh et al. [15] proved that is possible to extract modal information at high frequencies where the measurement is spoiled by noise. This is achieved by identifying the system poles with a high sensitivity sensor and, using those poles, performing the curve fitting of the frequency response functions from the optical system and determining the full-field mode shapes.

According to the limitations, using an appropriate model that describes the frequency response is even more relevant for the accurateness of the modal identification than with high sensitivity techniques. Conventionally, experimental modal analysis methods obtain the modal parameters from frequency response functions (FRF) [16], a transfer function between the displacement response and the force excitation. However, it is not always possible to perform tests for modal analysis in which the load can be measured. One special case is that in which excitation is applied as a motion in the base or support of the structure, which is transmitted to the system. This type of excitation is recommended for small and lightweight specimens, where applying and measuring the excitation force involves practical difficulties and alterations of mechanical behaviour. For those cases, the transfer function relates the motion of the measured degrees-of-freedom (DOF) of the structure and the motion of the base. This is known as the transmissibility function and its theoretical expression differs from the FRF's. Hence, although similar, modal parameters must not be obtained from transmissibility functions using conventional identification methods without a proper manipulation of the data [17]. In this sense, Chen et al. [18] employed a suitable modal model derived for base excitation to characterise the modal parameters of dragonfly wings using photonic probes and Ozdoganlar et al. [19] for microelectromechanical systems and the effect of ambient pressure on damping measuring with laser Doppler vibrometer.

Base excitation has been already employed with 3D-DIC measurements. Most studies simply measured operational deflection shapes, harmonically exciting one resonance to obtain maps similar to mode shapes [20–22]. Ha et al. performed a first approach to modal identification in an artificial beetle wing [23]. Natural frequencies were visually identified in the transfer function and damping ratios were estimated using the half-power method, but data was not manipulated according to base excitation. Then, they estimated mode shapes as an approximation to operational deflection shapes excited harmonically. On the other hand, Molina-Viedma et al. proposed a simple data manipulation of transmissibility functions, based on the mathematical relation with frequency response functions, for modal analysis using the circle-fit identification method in a cantilever beam [24], with simple geometry, and in a multi-component automotive lighting system [25]. In the mentioned cases, the methods employed were based on single-DOF models, which only analyses the vicinity of the resonances individually, neglecting the influence of the rest of the resonances. Only in the particular case of well-separated resonances, these methods can be valid. The rest of the curve, concerning the low-response spectrum with valleys and anti-resonances, is excluded from the fitting process. Therefore, to highlight the necessity of manipulating the vision measurement in base excitation test for general cases, multi-DOF fitting methods must be evaluated.

This work performs a study on the accuracy of modal identification on transmissibility functions where the full-field response is measured by 3D-DIC under base motion excitation. An adaptation of the transmissibility functions is performed to fit classical identification procedures based on frequency response functions fitting [17]. The comparison with the original transmissibility functions, as measured in the test, reveals how the modal model, obtained with this procedure, fits better the experimental measurements, especially concerning mode shapes and curve synthesis.

2. Mechanical response to base excitation

The response of a general mechanical system of N DOFs is defined by the following matrix-form equation [16]:

$$[M]\{\ddot{x}\} + [C]\{\dot{x}\} + [K]\{x\} = \{f(t)\} \tag{1}$$

where [M], [C] and [K] are the mass, damping and stiffness matrices of $N \times N$ size, $\{f\}$ is the external force vector and $\{x\}$ the displacement vector of each DOF, both $N \times 1$ vectors. Under harmonic excitation, this equation yields a system of second-order non-homogeneous linear differential equations, whose solution can be found to be also harmonic:

$$\{f(t)\} = \frac{1}{2}\{F\}e^{i\omega t} + \frac{1}{2}\{F^*\}e^{-i\omega t}$$

$$\{x(t)\} = \frac{1}{2}\{X\}e^{i\omega t} + \frac{1}{2}\{X^*\}e^{-i\omega t} \tag{2}$$

The transfer function between force magnitude, F, and displacement magnitude, X, depending on the harmonic term, ω, is known as frequency response function, being * the complex conjugate. It is a matrix, $[H]$, of $N \times N$ terms defined as follows:

$$\{X\} = [H]\{F\}$$

$$[H(i\omega)] = \sum_{k=1}^{m} \frac{[A_k]}{i\omega - \lambda_k} + \frac{[A_k^*]}{i\omega - \lambda_k^*} \tag{3}$$

where index m is the number of poles of the system, λ_k, i.e., the roots of the eigenproblem, which contain the natural frequency and damping information. A_k are the residues, from which mode shapes are obtained. This relation is the basis for experimental modal analysis, where FRFs are experimentally measured through the frequency-domain signals of displacements and loads.

When a mechanical system is subjected to motion excitation in its support, the absolute motion of each DOF coordinate, y, can be defined in terms of the base motion, z, and the relative motion of each DOF coordinate to the base, x, as:

$$\{y(t)\} = \{x(t)\} + z(t)\{g\}$$

$$\{\dot{y}\} = \{\dot{x}\} + \dot{z}\{g\}$$

$$\{\ddot{y}\} = \{\ddot{x}\} + \ddot{z}\{g\} \tag{4}$$

where $\{g\}$ is a vector function of the geometry, indicating how the motion of amplitude z affects each DOF. Using Newton's second law or Lagrange's equations, the governing equations for a system excited through the base are condensed in this matrix equation [17]:

$$[M]\{\ddot{x}\} + [C]\{\dot{x}\} + [K]\{x\} = -\ddot{z}[M]\{g\} \tag{5}$$

It is observed that the damping and stiffness forces, which depend on the relative motion between adjacent DOF, are defined by relative coordinates to the base frame. Conversely, inertial forces are proportional to the absolute motion. In the absence of external forces, the base motion term in the inertial forces,$\ddot{z}[M]\{g\}$, is seen as an equivalent external force and moved to the right side of the equation. This arrangement yields an analogous equation to eq. (1). If the base motion is expressed harmonically:

$$\{z(t)\} = \frac{1}{2}\{Z\}e^{i\omega t} + \frac{1}{2}\{Z^*\}e^{-i\omega t} \tag{6}$$

the magnitude of the equivalent force can be expressed as:

$$\{F\} = -\ddot{Z}[M]\{g\} \tag{7}$$

and, therefore,

$$\{X\} = -[H][M]\{g\}\ddot{Z} \tag{8}$$

Considering $\{g\}$ and $[M]$ as constants, it is found out that an FRF relating X and F is proportionally equivalent to the transmissibility function, $-[H][M]\{g\}$, between the relative motion to the base, X, and the magnitude of the base motion acceleration, $\ddot{Z}$.

2.1. Modal identification in base motion tests

According to eq. (3) and (8), transmissibility function has the same shape as FRF but with a different scale, depending on $\{g\}$ and $[M]$. The scaling factor is assumed by the residues, as illustrated by transmissibility functions in eq. (9), from where modal shapes are determined. Hence, the poles identification procedure gives the same results using any of these transfer functions. That is to say, damping and natural frequencies identification are indifferent in the movable or fixed base cases.

$$\frac{\{X\}}{\ddot{Z}} = \sum_{k=1}^{m} \frac{[A_k][M]\{g\}}{i\omega - \lambda_k} + \frac{[A_k^*][M]\{g\}}{i\omega - \lambda_k^*} \tag{9}$$

If $\{g\}$ and $[M]$ are known, the equivalent FRF matrix, $[H]$, can be deduced and non-scaled mode shapes are obtained by the modal identification methods based on eq. (3). Otherwise, the mode shapes are scaled by an unknown factor. In experimental modal analysis using base excitation, the latter is the most common case as, mainly, mass matrix representing the mass of each measured DOF in a continuum is hard to determine. However, as mode shapes magnitude has no physical significance, normalization is to be employed. Scaling affects the magnitude but not the relevant information: the shape, i.e., the proportionality between each DOF amplitude in a mode. Therefore, mode shapes are also the same for movable or fixed base.

Concluding, modal identification can be performed in base excitation test using FRF-based modal identification methods provided the transmissibility functions are determined as defined in eq. (8). Then, the synthetic transmissibility functions can be constructed using eq. (3) with the poles, λ_k, and the scaled residues, $[A_k][M]\{g\}$, obtained in the modal identification.

3. Experimental methodology

The experimental work intended to reveal the errors committed during the modal characterisation in absolute response transmissibility functions using FRF-based identification methods. Especially for vision techniques, like DIC, with a low signal-to-noise ratio in the valley regions of the response spectrum. To do this, modal analyses for absolute motion transmissibility functions and those

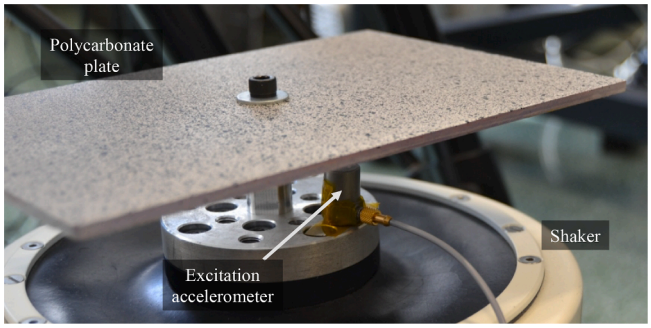

Fig. 1. Lay-out for the specimen mounted on the shaker's armature and accelerometer location for base motion measurement.

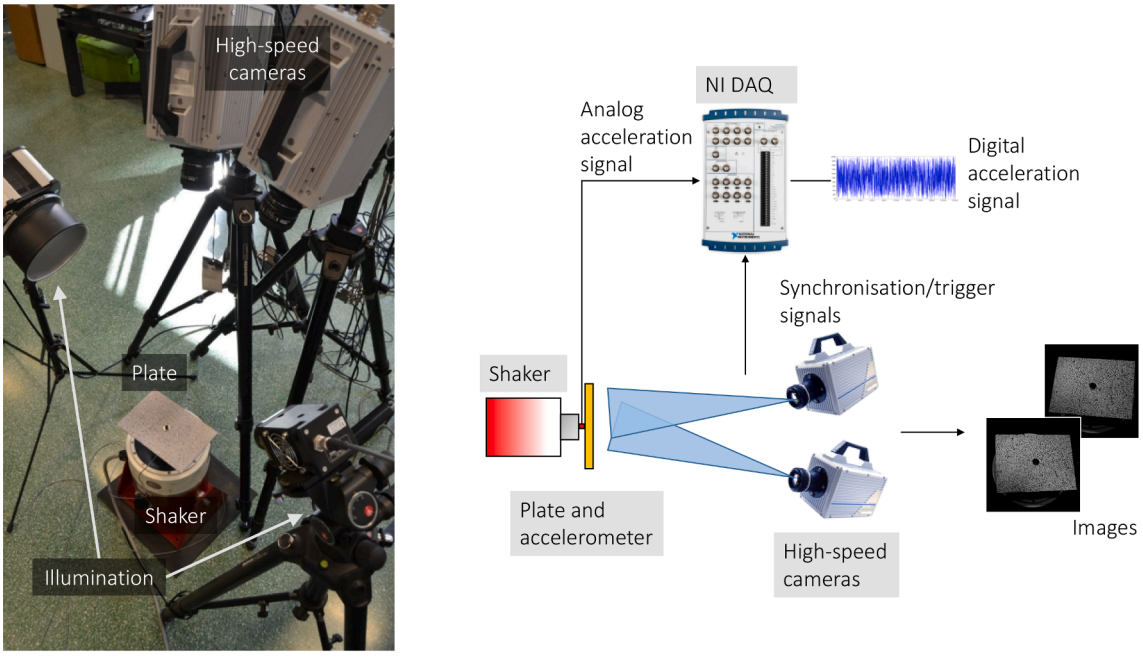

Fig. 2. (a) Picture of the experimental set-up and (b) measurement scheme.

defined in section 2, equivalent to FRFs, were compared through modal parameters and synthetic response curves reconstruction. Consolidated modal estimation algorithms were employed for this purpose. The whole procedure is described in the following subsections.

3.1. Experimental setup

To obtain representative experimental data for the modal identification, a rectangular polycarbonate plate was designed through a modal analysis in a finite element model to contain several modes in a frequency range suitable for vision measurements. Its dimensions were 210 mm in length, 140 mm in width and 4 mm in thickness. Experimentally, the plate was fixed at its central point to a shaker, model GW-V55/PA300E by DataPhysics, through a rigid joint, as illustrated in Fig. 1. In this way, the excitation motion of the shaker is transmitted to the plate through the joint, producing the characteristic base motion excitation. In this test, the response spectrum of the plate from 20 to 500 Hz was measured using a random excitation signal. The base excitation was registered by an accelerometer placed on the shaker's armature, as shown in Fig. 1. The response of the plate was measured using 3D-DIC. This technique performs tracking of subsets of the region of interest based on correlation criteria, for which every subset must be unique and identifiable [4]. For this purpose, a habitual procedure of specimen preparation was carried out, consisting in coating with a white paint background and, afterwards, adding black dots to make a random speckle pattern. A stereoscopic system consisting of two high-speed cameras (FastCam SA4 from Photron, 1 megapixel, 50 mm lenses,) was employed. A schematic layout of the setup is shown in Fig. 2.

Accomplishing with the Nyquist-Shannon theorem regarding the spectrum of analysis, the recording frame rate was 1000 fps. Moreover, the chosen exposure time of the sensor was 200 μs, which guarantees the instantaneity of the frames regarding the highest excitation frequency. Two light sources supplied the necessary illumination due to this short exposure. In total, two sequences of 5457 images each were recorded. A DAQ system (NI USB-6251 DAQ) was devoted to acquiring the accelerometer signal, synchronised with the high-speed cameras. Thus, a perfect correlation between response and excitation measurements was achieved.

The images were then processed using a commercial DIC algorithm, VIC-3D software by Correlated Solutions Inc. The surface of the specimen was divided into square subsets of 17 pixels, with a step between them of 9 pixels. As a result, a measurement grid of 6298 displacement sensors was achieved. For this work, only the out-of-plane displacements, perpendicular to the plate surface, were considered in the subsequent processing.

3.2. Transmissibility functions estimation

Once the response and excitation measurements were obtained in terms of absolute displacement and acceleration, respectively, the next step involved the calculation of the transfer function to be submitted to modal identification. All the necessary computations, described below, were performed by custom Python code. Welch's averaging method was employed to estimate the cross and auto power spectral density, S, from which the transfer function was obtained. The estimation in both captures were performed using 1000 samples long windows for averaging with a standard overlap of 50%. That yielded a frequency resolution of 1 Hz for the estimations of each sequence, which were eventually averaged to obtain a unique estimation of the whole test. The *H1* estimator for the transfer function was used for being less sensitive to noise in the output signal, considering that the sensitivity of DIC is much lower than the accelerometers:

$$T_{\text{abs}} = \frac{S_{\ddot{z}y}}{S_{\ddot{z}\ddot{z}}} \tag{10}$$

In the current case, this transmissibility function, T_{abs}, is defined as the relation between the absolute displacement of the response, y, measured by 3D-DIC, and the excitation acceleration, $\ddot{z}$, by the accelerometer. Hereafter, it is also referred to as the original dataset. In this form, it does not meet the conditions defined in section 2 for modal analysis, i.e., the transmissibility functions must be expressed in terms of relative displacement, x. The most straightforward way to estimate is as follow. First, the transmissibility in eq. (10) was transformed into a displacements ratio by integrating the excitation acceleration. In the frequency domain, it is equivalent to multiplying the function in eq. (10) by the vector of radian frequencies, ω^2. This form of transmissibility function would be directly obtained when using only sensors of the same type, for instance, accelerometers. Then, the estimation of the transmissibility function in terms of relative response to the excitation could be obtained according to the linear properties of the operations involved in the estimation of the power spectral density. Defining $F\{\}$ as the Fourier transform operator, relative motion transmissibility function, T_{rel}, can be simplified as:

$$\frac{F\{x\}}{F\{z\}} = \frac{F\{y-z\}}{F\{z\}} = \frac{F\{y\}}{F\{z\}} - 1$$

$$T_{\text{rel}} = T_{\text{abs}} - 1 \tag{11}$$

This means that by subtracting 1 from the absolute motion transmissibility function, it could be converted into the transmissibility function in terms of relative motion, both dimensionless. Finally, to get the transmissibility functions suitable for FRF-based modal identification, excitation had to be expressed back in terms of acceleration, so the previous integration was undone by dividing by ω^2.

3.3. Modal identification

Both the absolute and relative motion transmissibility functions were employed as input data for the characterisation of modal parameters using FRF-based methods. Namely, two standard procedures were considered in this work to neglect the influence of the identification method: the poly-reference least squares complex frequency (a.k.a. PolyMAX) [26] and the least-squares complex exponential (LSCE) [16], both implemented in LMS Testlab software by Siemens.

In the first step, the poles of the system, which contain the natural frequency and damping of the physical modes, were identified through the stability verification as the order of the model increases. A frequency band from 50 to 500 Hz was selected to exclude the non-excited spectrum and a spurious pole at 0 rad/s that appears in the absolute transmissibility functions. In the relative motion data, that pole is properly removed by the transformation.

Once the poles were extracted, a linear least-squares frequency-domain solver is used to obtain the residues in eq. (3) by fitting the curve to the given experimental transmissibility functions. In this step, mode shapes are defined. The effect of the modes over 500 Hz on the response was corrected by considering the upper residual during the fitting procedure. Conversely, the lower residual was omitted since no mode is below 50 Hz. Besides the estimation of the modal parameters, the synthetic transmissibility reconstruction through eq. (3) was assessed through the evaluation of the error and correlation between experimental and synthetic transmissibility, which revealed the level of accuracy of the curve fitting in both datasets:

$$Err = \frac{\sum_i (S_i - M_i)(S_i - M_i)^*}{\sum_i \left(S_i \cdot S_i^*\right)}$$

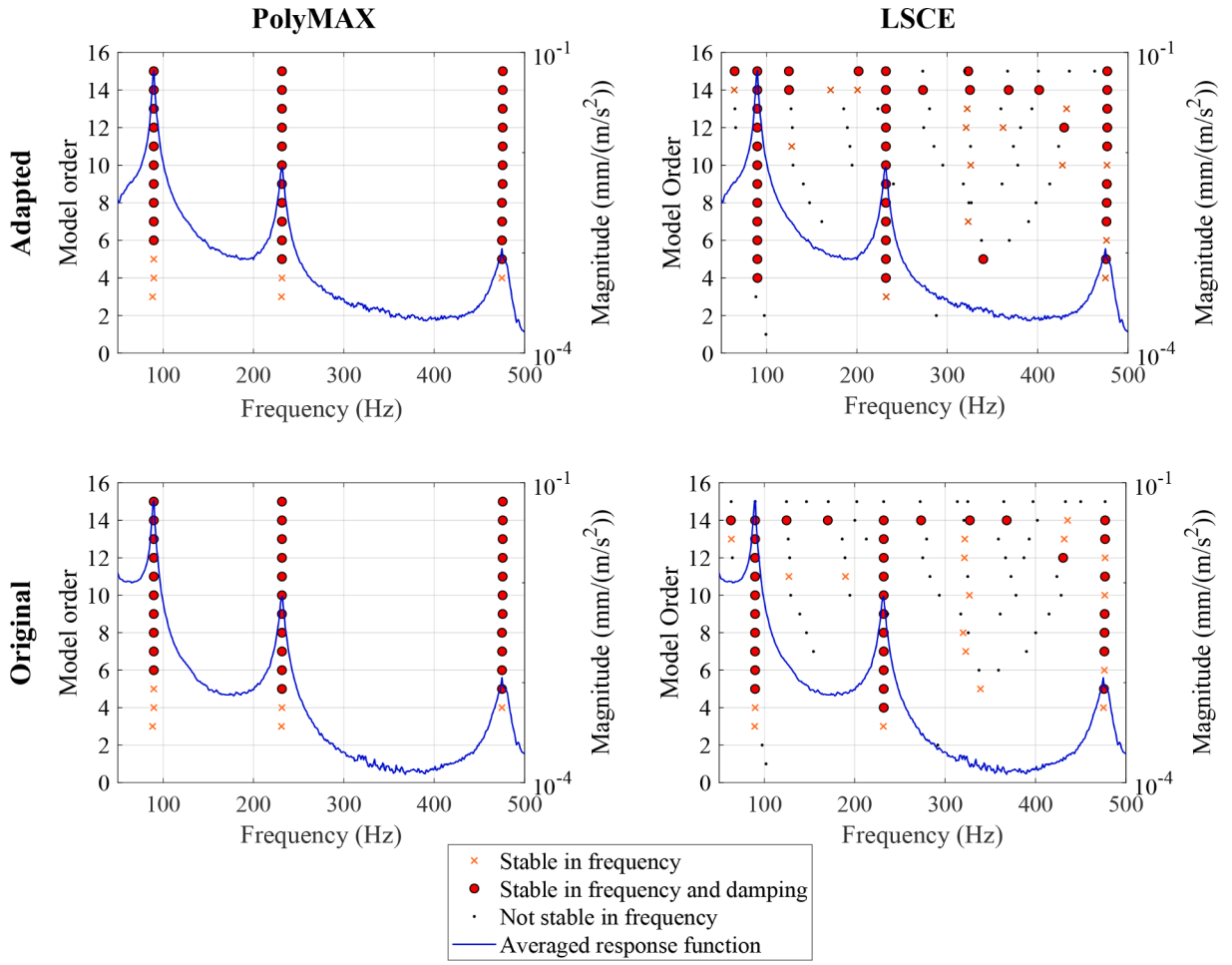

Fig. 3. Stabilisation diagrams for the adapted and the original transmissibility functions through the PolyMAX and LSCE procedures.

$$Corr = \frac{\left|\sum_i S_i \cdot M_i^*\right|^2}{\left(\sum_i S_i \cdot S_i^*\right)\left(\sum_i M_i \cdot M_i^*\right)} \tag{12}$$

Being S_i and M_i the complex value of the synthesised and measured function, respectively, at the spectral line i and * indicates complex conjugate.

4. Results

Along this section, the comments on the results are valid both for PolyMAX and LSCE identification procedures, unless specified, since they provide nearly identical results. Therefore, they are focused on the comparison between both datasets. As exposed above, the first step is the poles identification for adapted and the original sets of transmissibility functions. Considering the number of modes in the spectrum of analysis and all of them are suitably excited through this mean of excitation, poles quickly reach stability for low order models. Namely, a maximum order of 15 was chosen to evaluate the stability of poles, enough to identify the physical modes with a reduced presence of computational poles.

The resulting diagrams for each case can be observed in Fig. 3. Three resonances can be visually identified in the average function from each data set. Preliminarily, certain differences are observed between curves, more evident in the low-response regions between resonance peaks. It includes the low-frequency spectrum before the first resonance, which reveals the raising trend toward 0 Hz in the original transmissibility function, as a false pole. As explained before, the spectrum was truncated to exclude this effect during the curve fitting. With both transmissibility functions sets, the three modes are quickly stabilised at a model order of about six using both identification procedures. As expected, PolyMAX provides a clearer stabilization diagram, with no computational modes in this case. Just slight differences were found in the poles values between the adapted data and the original one. It can be observed in the resulting natural frequency and damping ratio values, in Table 1. These parameters are less sensitive to the shape of the adopted transmissibility functions.

Table 1
Natural frequencies and damping ratios obtained for the studied cases.

	Adapted data				Original data			
	Natural freq. (Hz)		Damping ratio		Natural freq. (Hz)		Damping ratio	
	PolyMAX	LSCE	PolyMAX	LSCE	PolyMAX	LSCE	PolyMAX	LSCE
Mode 1	89.673	89.616	1.40	1.30	89.703	89.666	1.31	1.31
Mode 2	231.562	231.579	1.01	1.01	231.559	231.576	1.01	1.01
Mode 3	475.657	475.331	0.98	1.02	475.273	475.387	0.87	0.99

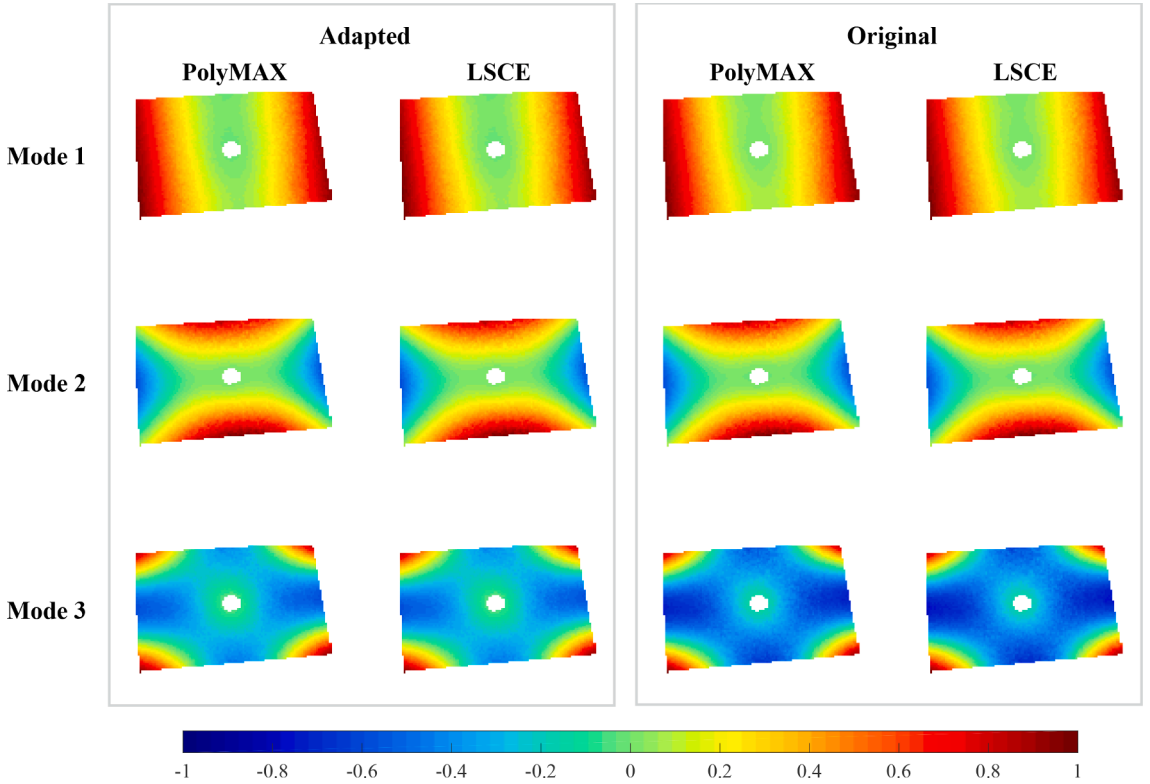

Fig. 4. Modal shapes obtained for the studied cases.

Using the identified poles, residues in eq. (3) were determined and mode shapes could be obtained. The resulting maps are shown in Fig. 4 for each case, using amplitude normalisation. They show up more clearly differences between datasets. Although in the first and second modes differences exist, they are still difficult to observe without an overlaid comparison, for instance. However, the third mode, with its more complex and stiffer shape, reveals the differences between the original and adapted functions. The most evident point is that the amplitude of the out-of-phase regions (in blue) are higher and wider in the original data. Another significant difference that must be highlighted occurs around the fixation. As can be observed for the adapted data, the amplitude of this region is about zero as indicates the green tone. However, in the original data identification the transition from dark to light blue does not reach green, which means that the amplitudes do not tend to zero as approaching the fixation. This incongruent result would indicate a poor fitting of the mode when the appropriate form of transmissibility functions is not employed, as exposed below. In addition, it must be considered that the original data represent the absolute response of the plate, so the response around the fixation tends to the base motion. In conclusion, using the absolute displacement estimation of transmissibility functions provides misleading mode shapes especially as the mode stiffness increases.

This observation leads to one of the main points of interest in this study, which is curve synthesis. The lower sensitivity of vision techniques regarding traditional methods is here particularly considered for the reconstruction of the response curves under base motion excitation. In Fig. 5, the synthesised response curves of two points are depicted along with the experimental curves. One point is located at the corner, where a high response is expected in most of the modes. The second one is placed in the middle of the right half of the plate. Overall, the low-response regions are poorly fitted in the original data. For instance, the adapted data have allowed for a better fitting of the low-frequency spectrum, below the first mode, as seen for both points. It also allowed the appropriate representation of the anti-resonance before the second mode at the corner point. Moreover, false anti-resonances around the third resonance peak are described for both points by the synthesised curve of the original data. Besides these deficiencies, a remarkable behaviour is

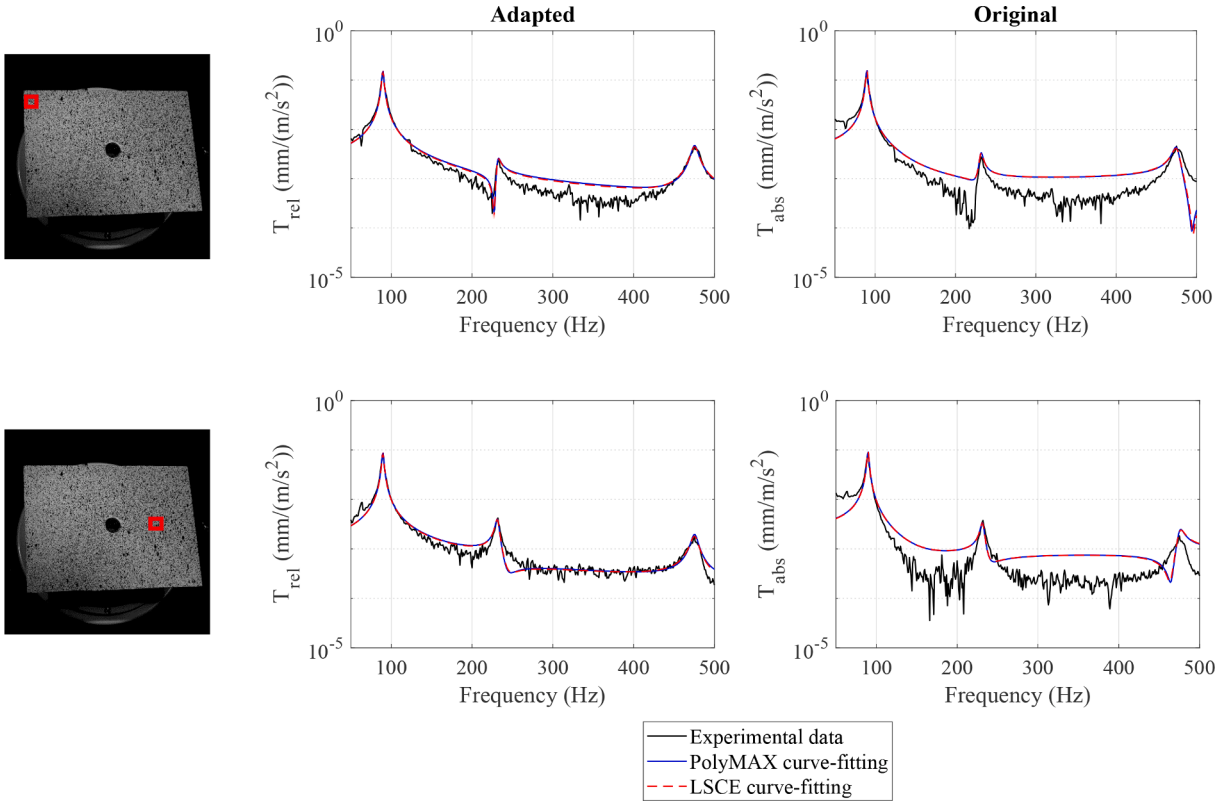

Fig. 5. Evaluation of the curve synthesis in both data sets at two different measurement points.

observed in the second plotted point regarding the third mode fitting. Whereas the peak amplitude is properly described for the adapted data, the amplitude of the synthesised curve in the original data is noticeable higher than the experimental. It should be noted that this point is placed in the region where the highest differences between the third mode estimations took place, according to Fig. 4. Therefore, it reveals that the difference is an overestimation of the third mode amplitude in these regions due to the non-suitable shape of the original curves for the FRF-based procedures.

After the evaluation at single measurement points, the analysis of these errors can exploit the full-field information to give new remarks. Besides the representation of high spatial resolution mode shapes, it allows evaluating the distribution across the specimen of quality indicators of the modal identification. Namely, the curve-fitting accuracy was evaluated through the correlation coefficient and the error between synthesised and experimental curves at every single measurement point, according to eq. (12). The result is depicted as 3D surfaces in Fig. 6. In both data sets, a common trend is observed: higher correlation and lower error are achieved in the furthest areas from the fixation, prone to develop a higher response. Taking PolyMAX results for illustration, the maximum correlation and the minimum error is achieved in the corners, with similar values for both data set: 98.8% and 97.8% correlation and 1.2% and 2.3% error for the adapted and the original sets, respectively. Although the difference is small, the adapted transmissibility functions allow for more accurate fitting. Then, the correlation falls and the error raises exponentially as approaches the fixation, where the lowest displacements occur. The error beside the fixation reaches values about 86% in both data sets. However, the correlation coefficient is lower for the original data, 23.4%, than for the adapted data, 30.1%. Beyond those contours of the plate, the curve-fitting statistical indicators are significantly worse in the original transmissibility functions, in general. Only 51% of the measurement points achieved a correlation over 90% and an error lower than 10%. Conversely, for the adapted data, this is achieved by the 73% of the measurement points. Hence, the adapted data reduce the points with more deficient indicators and concentrate them in a narrower area around the fixation. This highlights the necessity of the transmissibility functions adaptation to obtain more accurate identifications. Considering the lower sensitivity of vision techniques, this is especially relevant in the low-amplitude areas.

5. Conclusions

This study addresses the analysis of the validity of the FRF-based procedures for modal identification for base excitation tests using vision techniques. It is motivated by the increasing popularity of those techniques for their contactless full-field measurements but with a lower sensitivity regarding traditional transducers, which reduces the accuracy of the identification and synthesis of the modal behaviour. Moreover, base motion excitation is quite common in practice and requires specific treatment for the analysis.

Experimental measurements were performed with 3D-DIC to determine the full-field transmissibility functions of a plate. After

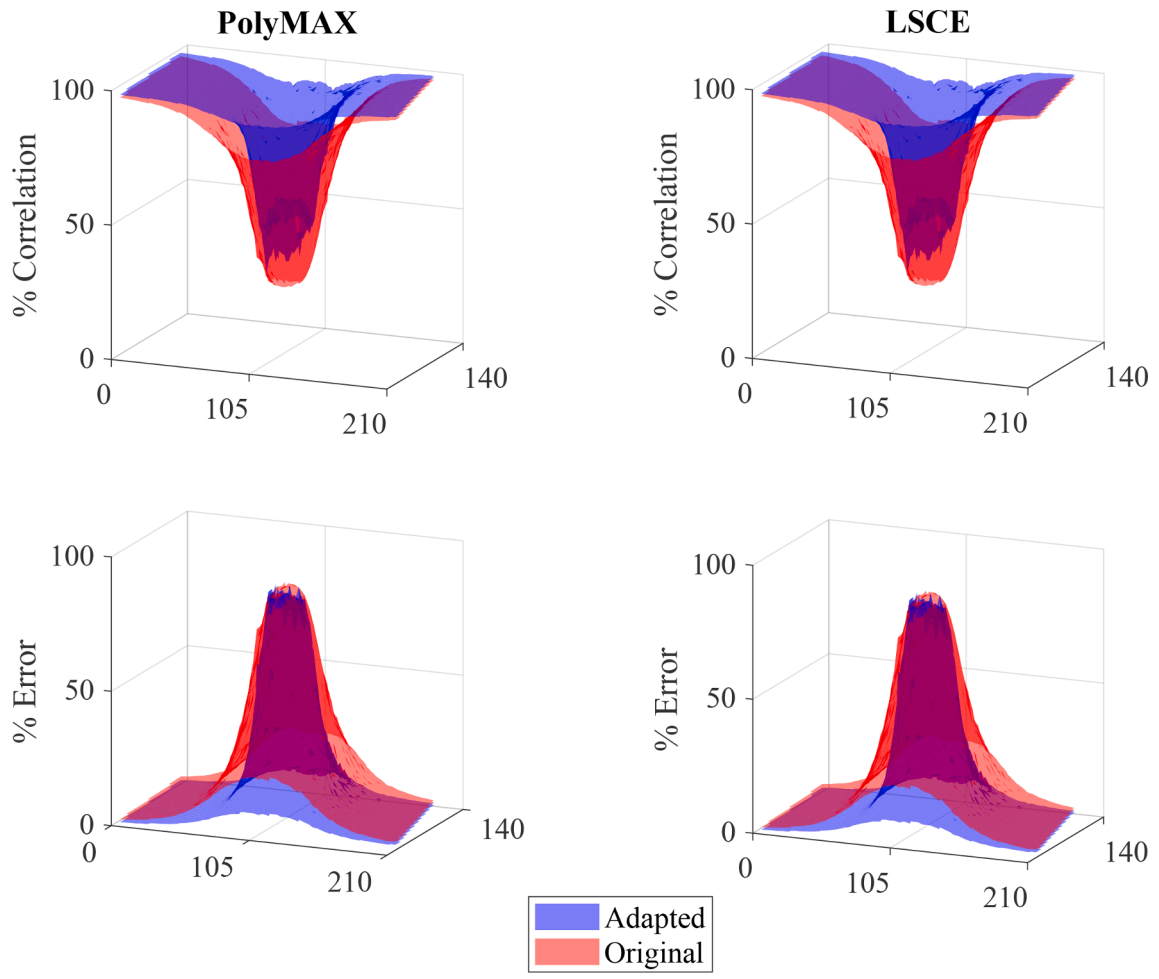

Fig. 6. Maps of the correlation coefficient and error value of the curve-fitting procedures for the adapted and original transmissibility functions.

performing the proper adaptation of the transmissibility functions for FRF-based procedures, modal analysis was performed using two of the best-known modal identification procedures: PolyMAX and LSCE.

The adapted transmissibility functions provide substantially better results in modal identification, particularly in regions close to the movable base, where the amplitude of displacements is lower and, hence the signal-to-noise ratio higher. Natural frequencies and damping ratios, as unique global parameters obtained from the poles of the system, are less affected by this fact and both datasets provide similar results. However, it has been proved that using improper transmissibility functions yields misleading mode shapes, especially for stiffer modes. It has been shown that this is due to poor curve fitting of the transmissibility functions.

The accuracy of the fitting was always higher for the adapted data, checked out through the correlation coefficient and the error between the synthesised curve and the experimental. The statistical parameters in the original data were poor in a wide area of the specimen. However, the adaptation reduces the poor-fitted areas to narrow regions around the base, just the region of lower displacements, improving the identification of mode shapes and the curves synthesis. These conclusions can be made independently of the identification procedure, as both of the employed yielded quite similar results. Hence, this analysis remarks the necessity of the adaptation of the response functions obtained with vision techniques for base excitation tests for accurate modal identification and synthesis with FRF-based procedures.

Declaration of Competing Interest

The authors declare that they have no known competing financial interests or personal relationships that could have appeared to influence the work reported in this paper.

Acknowledgement

This work was supported by the Andalusian Government [grant numbers 1263076, P20_00312].

References

[1] J. Baqersad, P. Poozesh, C. Niezrecki, P. Avitabile, Photogrammetry and optical methods in structural dynamics – A review, Mech. Syst. Signal Process. 86 (2017) 17–34, https://doi.org/10.1016/j.ymssp.2016.02.011.

[2] W. Wang, J.E. Mottershead, A. Ihle, T. Siebert, H. Reinhard Schubach, Finite element model updating from full-field vibration measurement using digital image correlation, J. Sound Vib. 330 (2011) 1599–1620, https://doi.org/10.1016/j.jsv.2010.10.036.

[3] M. Cuadrado, J. Pernas-Sánchez, J.A. Artero-Guerrero, D. Varas, Model updating of uncertain parameters of carbon/epoxy composite plates using digital image correlation for full-field vibration measurement, Measurement. 159 (2020), 107783, https://doi.org/10.1016/j.measurement.2020.107783.

[4] H. Schreier, J.-J. Orteu, M.A. Sutton, Image Correlation for Shape, Motion and Deformation Measurements, Springer US, Boston, MA, 2009. Doi: 10.1007/978-0-387-78747-3.

[5] F. Trebuňa, M. Hagara, Experimental modal analysis performed by high-speed digital image correlation system, Measurement. 50 (2014) 78–85, https://doi.org/10.1016/j.measurement.2013.12.038.

[6] Á.J. Molina-Viedma, L. Felipe-Sesé, E. López-Alba, F.A. Díaz, Comparative of conventional and alternative Digital Image Correlation techniques for 3D modal characterisation, Measurement. 151 (2020), 107101, https://doi.org/10.1016/j.measurement.2019.107101.

[7] R. Huňady, M. Hagara, A new procedure of modal parameter estimation for high-speed digital image correlation, Mech. Syst. Signal Process. 93 (2017) 66–79, https://doi.org/10.1016/j.ymssp.2017.02.010.

[8] A. Zanarini, Full field optical measurements in experimental modal analysis and model updating, J. Sound Vib. 442 (2019) 817–842, https://doi.org/10.1016/j.jsv.2018.09.048.

[9] Y.-H. Chang, W. Wang, J.-Y. Chang, J.E. Mottershead, Compressed sensing for OMA using full-field vibration images, Mech. Syst. Signal Process. 129 (2019) 394–406, https://doi.org/10.1016/j.ymssp.2019.04.031.

[10] D. Uehara, J. Sirohi, Full-field optical deformation measurement and operational modal analysis of a flexible rotor blade, Mech. Syst. Signal Process. 133 (2019), 106265, https://doi.org/10.1016/j.ymssp.2019.106265.

[11] Y. Hu, W. Guo, W. Zhu, Y. Xu, Local damage detection of membranes based on Bayesian operational modal analysis and three-dimensional digital image correlation, Mech. Syst. Signal Process. 131 (2019) 633–648, https://doi.org/10.1016/j.ymssp.2019.04.051.

[12] Á. Molina-Viedma, E. López-Alba, L. Felipe-Sesé, F. Díaz, Full-Field Operational Modal Analysis of an Aircraft Composite Panel from the Dynamic Response in Multi-Impact Test, Sensors. 21 (2021) 1602, https://doi.org/10.3390/s21051602.

[13] C. Warren, C. Niezrecki, P. Avitabile, P. Pingle, Comparison of FRF measurements and mode shapes determined using optically image based, laser, and accelerometer measurements, Mech. Syst. Signal Process. 25 (2011) 2191–2202, https://doi.org/10.1016/j.ymssp.2011.01.018.

[14] P.L. Reu, D.P. Rohe, L.D. Jacobs, Comparison of DIC and LDV for practical vibration and modal measurements, Mech. Syst. Signal Process. 86 (2017) 2–16, https://doi.org/10.1016/j.ymssp.2016.02.006.

[15] J. Javh, J. Slavič, M. Boltežar, High frequency modal identification on noisy high-speed camera data, Mech. Syst. Signal Process. 98 (2018) 344–351, https://doi.org/10.1016/j.ymssp.2017.05.008.

[16] D.J. Ewins, Modal Testing: Theory, Practice, and Application, 2nd ed., Research Studies Press LTD, Baldock, Hertfordshire, England, 2000.

[17] J.G. Béliveau, F.R. Vigneron, Y. Soucy, S. Draisey, Modal parameter estimation from base excitation, J. Sound Vib. 107 (1986) 435–449, https://doi.org/10.1016/S0022-460X(86)80117-1.

[18] J.S. Chen, J.Y. Chen, Y.F. Chou, On the natural frequencies and mode shapes of dragonfly wings, J. Sound Vib. 313 (2008) 643–654, https://doi.org/10.1016/j.jsv.2007.11.056.

[19] O.B. Ozdoganlar, B.D. Hansche, T.G. Carne, Experimental Modal Analysis for Microelectromechanical Systems, Exp. Mech. 45 (2005) 498–506, https://doi.org/10.1177/0014485105059991.

[20] N.S. Ha, T. Jin, N.S. Goo, Modal analysis of an artificial wing mimicking an Allomyrina dichotoma beetle's hind wing for flapping-wing micro air vehicles by noncontact measurement techniques, Opt. Lasers Eng. 51 (2013) 560–570, https://doi.org/10.1016/j.optlaseng.2012.12.012.

[21] A.J. Molina-Viedma, L. Felipe-Sesé, E. López-Alba, F.A. Díaz, 3D mode shapes characterisation using phase-based motion magnification in large structures using stereoscopic DIC, Mech. Syst. Signal Process. 108 (2018) 140–155, https://doi.org/10.1016/j.ymssp.2018.02.006.

[22] P. Neri, A. Paoli, A.V. Razionale, C. Santus, Low-speed cameras system for 3D-DIC vibration measurements in the kHz range, Mech. Syst. Signal Process. 162 (2022), 108040, https://doi.org/10.1016/j.ymssp.2021.108040.

[23] N.S. Ha, H.M. Vang, N.S. Goo, Modal Analysis Using Digital Image Correlation Technique: An Application to Artificial Wing Mimicking Beetle's Hind Wing, Exp. Mech. 55 (5) (2015) 989–998.

[24] Á.J. Molina-Viedma, E. López-Alba, L. Felipe-Sesé, F.A. Díaz, Full-field modal analysis during base motion excitation using high-speed 3D digital image correlation, Meas. Sci. Technol. 28 (10) (2017) 105402.

[25] Á. Molina-Viedma, E. López-Alba, L. Felipe-Sesé, F. Díaz, Modal Identification in an Automotive Multi-Component System Using HS 3D-DIC, Materials (Basel). 11 (2018) 241, https://doi.org/10.3390/ma11020241.

[26] P. Guillaume, P. Verboven, S. Vanlanduit, H. Van Der Auweraer, B. Peeters, A poly-reference implementation of the least-squares complex frequency-domain estimator, Proc. IMAC. 21 (2003) 183–192.